EPJ Web of Conferences **36**, 00006 (2012)
DOI: 10.1051/epjconf/20123600006

Light vector mesons and the dielectron continuum in PHENIX

Sarah Campbell[1,a] for the PHENIX Collaboration

[1]Iowa State University

Abstract. The PHENIX experiment at RHIC has measured the dielectron continuum and the ω and ϕ light vector mesons using hadronic and dielectron decay channels in $\sqrt{s_{NN}}$ = 200 GeV p+p, d+Au, Cu+Cu and Au+Au collisions. The ω and ϕ mesons experience no strong cold nuclear matter effects but in central heavy ion collisions their yields are suppressed at high p_T, extending to intermediate p_T for the ϕ. The comparison of the ω and ϕ suppression to the suppression of other hadrons suggests parton energy loss for high p_T mesons and favors a recombination production mechanism for intermediate p_T ϕ mesons. The dielectron continuum shows a low mass excess in central Au+Au and Cu+Cu collisions while the p+p and d+Au spectra agree with their respective cocktails. The low mass excess consists of a high p_T thermal virtual photon component and a much larger low p_T component.

1 Introduction

Hadrons produced in relativistic heavy ion collisions provide a mechanism to study the quark gluon plasma. This proceeding discusses PHENIX's ω and ϕ light vector mesons measurements from both hadronic and dielectron decays and the dielectron continuum spectra that provides access to the ρ spectral function. The light vector mesons (ω, ϕ, ρ) are predicted to undergo mass and/or width modifications by the medium created in the collision [1] and broadening of the ρ spectral line shape was measured by NA60 at SPS [2]. The dielectron decays of vector mesons provide electro-magnetic signals without color charge that are not modified by the final state and sample a large time window during the collision's evolution. With both the dielectron and hadron decay channels of the ω and ϕ, we can extend the transverse momentum, p_T, range of the measurements and compare decay channels to identify possible variations due to medium effects.

The nuclear modification factor, R_{AA}, of the ω and ϕ in heavy ion collisions provides insight into energy loss and particle production mechanisms. R_{AA}, Equation 1, is the ratio of the heavy ion spectrum to a p+p reference spectrum scaled by the average number of binary collisions, N_{Coll}.

$$R_{AA}(p_T) = \frac{d^2N_{AA}/dydp_T}{\left(N_{Coll}/\sigma_{pp}^{inel}\right) \times d^2\sigma_{pp}/dydp_T} \tag{1}$$

where $d^2N_{AA}/dydp_T$ is the differential yield per event in A+A collisions, σ_{pp}^{inel} is the total inelastic p+p cross-section, and $d^2\sigma_{pp}/dydp_T$ is the differential p+p cross-section. In heavy ion collisions, a factor of five suppression of the π^0 and η meson production with respect to the p+p scaled by the average number of binary collisions is seen [3] [4]. Protons [5] and other baryons [6] [7] do not experience this suppression particularly at intermediate p_T where they are enhanced relative to binary scaled p+p collisions. Since the ω meson has the same quark content as the π^0 but with a larger mass and intrinsic spin, it's behavior can provide more information on energy loss in the quark gluon plasma. The ϕ meson is a $s\bar{s}$ state with a mass similar to the proton, it can also answer questions of energy loss and baryon-meson differences.

[a] e-mail: campbels@iastate.edu

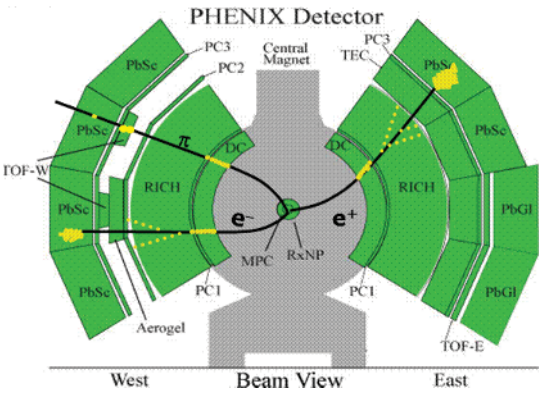

Fig. 1. The beam view of the central arms of the PHENIX detector with example tracks for a positron, an electron, and a charged pion.

First the PHENIX central arm detectors are presented. Then PHENIX ω and ϕ measurements are discussed. This is followed by PHENIX's dielectron continuum measurements and a brief conclusion.

2 PHENIX detector

The central arms of the PHENIX detector, shown in Figure 1, consist of two spectrometers each with spanning $\pi/2$ in azimuth and ± 0.35 in pseudorapidity. Charged particles bent by the magnetic field are tracked in the drift chamber (DC) and first pad chamber (PC1) with a momentum resolution of $\delta p/p = 0.7\% \oplus 1.1\% p$ [GeV/c] [8]. Two electro-magnetic calorimeters (PbSc and PbGl) measure photons and reconstruct photon pairs from π^0 and η decays. Electrons are identified by a Cherenkov ring in the ring imaging Cherenkov detector (RICH) and an electro-magnetic shower in the PbGl and PbSc. Particle identification of charged hadrons is possible using the momentum from the DC and PC1 and the time of flight information from the time-of-flight (TOF) and aerogel detectors. The TOF-East is used for kaon identification in the $\phi \rightarrow K^+K^-$ channel presented in Section 3. It has a time resolution of 120 ps and a π/K separation in the p_T range 0.3-2.2 GeV/c [9]. Beam-beam counters and zero degree calorimeters are located around the beam pipe to the north and south of the central arms [10]. They determine the position of the collision along the beam axis and the collision's centrality, a measure of the collision's nuclear overlap.

3 The ϕ and ω mesons

The ϕ and ω mesons are measured in $s_{NN} = \sqrt{200}$ GeV p+p, d+Au, Cu+Cu and Au+Au collisions with a variety of decay channels, presented in Table 1. Raw yields are corrected for the acceptance and reconstruction efficiency, embedding efficiency to correct for occupancy effects, trigger bias or efficiency effects, and the decay's branching ratio. By measuring the ϕ and ω p_T spectra in different channels the p_T range is extended. A smooth transition from the dielectron decays at low p_T to the hadronic decays at high p_T is seen with overlap in the intermediate p_T range where they agree. This agreement is seen in the ϕ from 1 to 3 GeV/c in p+p collisions, from 1 to 5 GeV/c in d+Au [11] and Au+Au collisions and in the ω from 2 to 4 GeV/c in p+p collisions and from 2 to 6 GeV/c in d+Au collisions [12].

3.1 Nuclear modification

d+Au collisions provide access to initial state cold nuclear matter effects, while heavy ion collisions such as Cu+Cu and Au+Au generate additional medium effects from the quark gluon plasma. The nuclear modifications of d+Au, Cu+Cu and Au+Au spectra are calculated by taking the ratio to the

Table 1. ϕ and ω meson decays measured in various collision systems.

p+p	d+Au	Cu+Cu	Au+Au
$\phi \to e^+e^-$	$\phi \to e^+e^-$	$\phi \to e^+e^-$	$\phi \to e^+e^-$
$\phi \to K^+K^-$	$\phi \to K^+K^-$	$\phi \to K^+K^-$	$\phi \to K^+K^-$
$\omega \to e^+e^-$	$\omega \to e^+e^-$	$\omega \to e^+e^-$	$\omega \to e^+e^-$
$\omega \to \pi^0\gamma$	$\omega \to \pi^0\gamma$	$\omega \to \pi^0\gamma$	$\omega \to \pi^0\gamma$
$\omega \to \pi^+\pi^-\pi^0$	$\omega \to \pi^+\pi^-\pi^0$		

p+p spectrum scaled by N_{Coll}, where N_{Coll} is calculated using a Glauber Monte Carlo simulation. When there are no nuclear effects this nuclear modification factor, R_{AA} (Equation 1) or R_{dA}, is one. A nuclear enhancement generates values greater than one and a suppression leads to values of less than one. The R_{dA} quantizes the cold nuclear matter effects in d+Au collisions relative to N_{Coll}-scaled p+p. Figure 2 shows the R_{dA} as a function of p_T for ω and ϕ mesons in central 0-20%, peripheral 60-88% and minimum bias (MB) d+Au collisions. For comparison these are shown with R_{dA} for π^0, η, η', K_S and protons. No strong cold nuclear matter effects are seen for the ω or ϕ mesons. No meson species dependence of R_{dA} is seen within the uncertainties. The peripheral d+Au meson spectra are consistent with the N_{Coll} scaled p+p spectra. For central d+Au collisions at intermediate p_T, there is little to no Cronin enhancement of ω, ϕ and π^0 mesons. A small suppression of ω and π^0 at p_T above 8 GeV/c is seen. The high p_T R_{dA} behavior of the ω and π^0 mesons suggests that there may be a small energy loss at the parton level given the similarity of the R_{AA} despite different meson masses [12].

Heavy ion collisions consider R_{AA} to identify modifications from the hot dense plasma created in the collision. Figure 3 presents the R_{AA} of ϕ and ω mesons in central Au+Au collisions as a function of p_T. The π^0, η, K^+, J/ψ, direct photon, proton and non-photonic electrons are shown for comparison. π^0 and η mesons have a factor of five suppression at high p_T. At p_T above 5 GeV/c, the ϕ and ω mesons show a flat suppression coincident with π^0 suppression. As the p_T is lowered the R_{AA} of the ϕ increases, the intermediate p_T behavior of the ϕ is similar to what is seen for K^+, another strange quark meson [5].

The suppression patterns seen in the central Au+Au collisions are also apparent in mid-central Au+Au and Cu+Cu collisions. The R_{AA} as a function of p_T in Cu+Cu and Au+Au collisions are compared for systems with the same number of participating nucleons, N_{Part}. The suppression of the ω at high p_T agrees with the level of π^0 suppression in both Cu+Cu and Au+Au collisions at intermediate N_{Part}. Similarly, in intermediate N_{Part} Cu+Cu and Au+Au collisions, the ϕ suppression at intermediate p_T, 2-5 GeV/c, remains above the π^0 and below the proton. At p_T above 5 GeV/c for the same collisions, the ϕ suppression agrees with the π^0 suppression. For both intermediate p_T ϕ and high p_T ω the N_{Part} dependence of the integrated R_{AA} is consistent in Cu+Cu and Au+Au collisions despite different collision geometries.

In peripheral collisions, ω and ϕ mesons are consistent with binary scaling. The ϕ is also consistent with a small enhancement seen in the peripheral proton R_{AA} [11]. The integrated R_{AA} for high p_T ω mesons as a function of N_{Part} shows that the suppression starts at a N_{Part} of 34 and increases with N_{Part}, a trend similar to the π^0 and η suppression. This high p_T R_{AA} vs N_{Part} dependence is fit with a fractional energy loss function, $R_{AA} = (1 - S_0 N_{Part}^a)^{n-2}$, with the n parameter fixed to eight. The resulting a parameter is consistent with PQM [13] and GLV [14] model predictions of a roughly $N_{Part}^{2/3}$ dependence. The similar suppression patterns seen in π^0, η and ω mesons at high p_T suggests that energy loss in the medium occurs at the parton level [15].

Understanding the intermediate ϕ suppression behavior is more difficult. Radial flow effects are unlikely causes of the ϕ suppression because of the different behaviors of the ϕ and proton which have similar masses, while the ϕ and K^+ are similarly suppressed even though kaons have less mass. Recombination may account for the ϕ and K^+ behavior because of their strangeness content. Given strangeness enhancement, there may be more thermal partons in strange meson production in a recombination scenario. This could result in an extension of soft processes out to higher p_T for strange mesons [11].

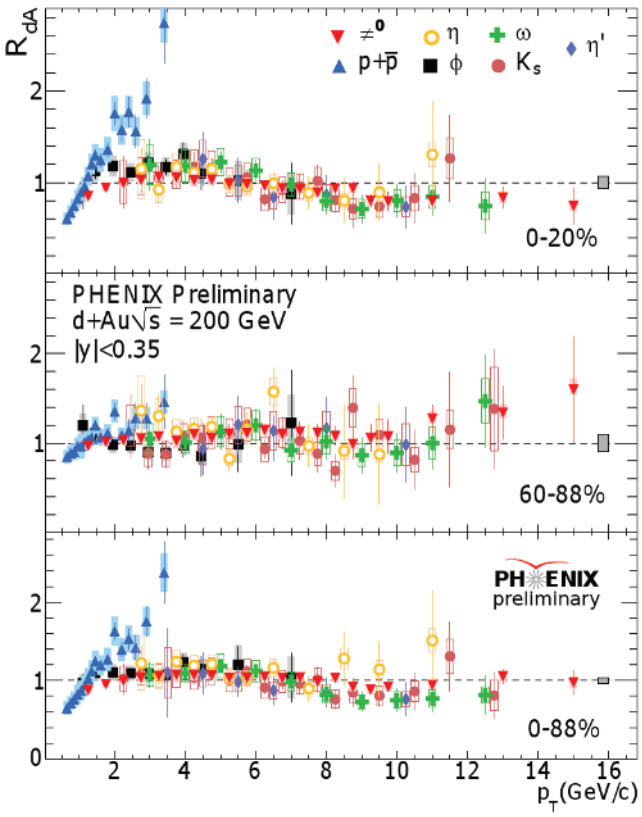

Fig. 2. The R_{dA} vs p_T for particles in 0-20%, 60-88% and MB (i.e. 0-88%) d+Au collisions. π^0, η, η', ω, ϕ, K_S and $p + \bar{p}$ are shown. The grey band around one provides the systematic error on the R_{dA} from the uncertainty in N_{Coll} for each plot.

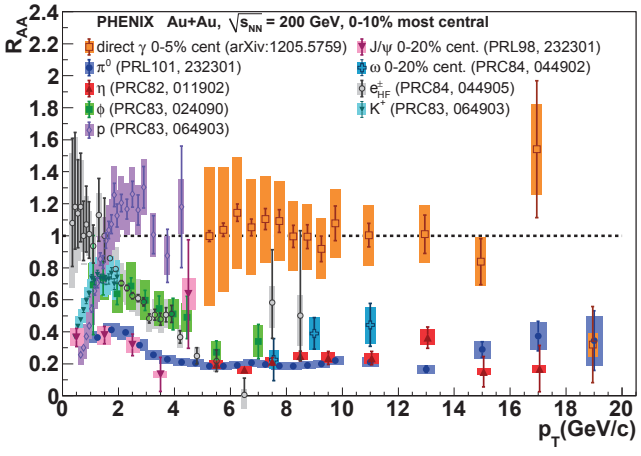

Fig. 3. The R_{AA} vs p_T for various particles in Au+Au central collisions. The π^0, η, ω, ϕ, K^+, proton, J/ψ, direct γ and non-photonic electrons or $e^{\pm}_{HF}$ are shown. These particles are from 0-10% Au+Au collisions except for the direct photons which are from 0-5% Au+Au and the ω and J/ψ which are from 0-20% Au+Au.

4 Dielectron continuum

NA60 measured the dielectron continuum in 158 AGeV In+In collisions at SPS and found the ρ to be broadened without a mass shift [2]. The ρ is a prime signal to identify mass modifications because of it's short lifetime, 2.1 fm/c. As a consequence, the ρ meson is more likely to decay in the medium. In a dielectron decay, an the electron-positron pair produced in medium will escape with no final state effects because leptons contain no color charge. However, the short lifetime of the ρ also means that it has a broad mass distribution. This combined with the decays of neighboring mesons make it difficult to isolate the ρ meson in a mass spectrum. By measuring the dielectron continuum, deviations in the mass spectrum due to ρ modification can be identified. Since the dielectron continuum contains information collected over the full time evolution of the medium, additional physics signals are present in the dielectron continuum. These include direct virtual photons, hadron Dalitz (π^0, η, η') and leptonic (ω, ϕ, J/ψ) decays, and correlations from electron-positron pairs resulting from semi-leptonic decays of open heavy flavor mesons correlated by the pair production of heavy quarks.

4.1 Cocktail

A reference cocktail of the expected hadronic sources is generated to compare the data to the expected physics signals. This is done using EXODUS, a hadronic decay generator. EXODUS handles the decay kinematics for two- and three-body hadron decays and the dielectron pair spectrum is determined. It is parameterized with measured PHENIX data including meson-to-pion ratios and a fit to the pion p_T spectrum with a modified Hagedorn exponential, Equation 2 where A, a, b, n, and p_0 are fit parameters [16].

$$E\frac{d^3\sigma}{dp^3} = A\left(e^{-\left(ap_T+bp_T^2\right)} + p_T/p_0\right)^{-n} \tag{2}$$

The p_T spectra of the other mesons are extrapolated assuming m_T scaling. The m_T scaling assumption is confirmed for the ϕ but deviations are seen at the higher mass J/ψ; the measured J/ψ p_T distribution is used instead. Additionally, meson-to-pion ratios are adjusted to reflect the suppression measured in heavy ion collisions and the J/ψ and ψ' line shapes are altered to include radiative tails. The PHENIX cocktail includes electron-positron pairs from vacuum ρ decays; additional dielectron yields due to ρ production via π-π annihilation are not included.

Dielectron correlations in the mass spectrum from heavy quarks and Drell-Yan are calculated with PYTHIA. In the p+p case, the dielectron spectrum is precise enough to subtract the hadronic components and measure the charm cross section. A charm cross section of 544 ± 39($stat$) ± 142(sys) ± 200($model$) μb was determined by fitting the PYTHIA line shapes for the charm and bottom and Drell-Yan components [17]. This agrees with the non-photonic single electron cross section of 567 ± 57($stat$) ± 193(sys) μb [18]. The heavy quark and Drell-Yan line shapes in p+p are scaled by the average number of collisions, N_{Coll}, for d+Au, Cu+Cu and Au+Au collisions. As a comparison a randomly correlated $c-\bar{c}$ spectrum is also generated using the PYTHIA single electron p_T spectrum and a randomly oriented opening angle between the electron-positron pairs [16]. The hadronic components from EXODUS and the heavy quark and Drell-Yan correlations are filtered in to the ideal PHENIX acceptance.

4.2 Analysis

To measure the dielectron continuum, backgrounds pairs must be removed. Backgrounds from conversions and detector effects such as RICH ring overlap are removed with pair cuts such as the ϕ_V cut and a ring separation cut respectively [16]. The remaining three backgrounds cannot be removed with cuts, they are statistically subtracted. The largest background source is the combinatorial background; the shaped of the combinatorial background is generated for like- and unlike-sign pairs by event mixing using a rolling buffer method. Background pairs from double Dalitz decays and hadronic decays with multiple electron-positron pairs create combinatorial pairs that are correlated from the original

parent hadron and are not included in the hadronic cocktail generated by EXODUS. These pairs, from pion double Dalitz decay and $\eta \to \pi\pi\pi$ decays with multiple pion Dalitz decays, are considered background and can be statistically subtracted from the analysis. The like- and unlike-sign line shapes of these decays are simulated using an EXODUS-like code that is able to make pairs from multiple electron-positron pair decay chains. Jets are the remaining source of background since multiple pions within a jet may Dalitz decay creating lepton pairs that are correlated through the jet kinematics. The jet background is simulated using PYTHIA. Both the jet and double Dalitz backgrounds create unlike- and like-sign pairs at the same rates as a result of the pair production of leptons.

The combinatorial, double Dalitz and jet backgrounds can be removed with either of two subtraction methods. This first method is a component by component subtraction that uses the like-sign pairs to find the relative contributions of the three remaining backgrounds. The simulated backgrounds are then subtracted from unlike-sign spectrum. The second background subtraction method is like-sign subtraction where an acceptance correction has been applied to the like-sign pairs. This is done by adjusting the like-sign pair spectrum differentially in mass and pair p_T to mimic the unlike-sign pair acceptance and then subtracting the like-sign pairs from the unlike-sign pairs. In p+p, Cu+Cu and Au+Au these two subtraction methods are performed separately and are consistent. The d+Au results are obtained with the acceptance corrected like-sign subtraction method.

After the backgrounds are subtracted the spectrum is corrected for the reconstruction efficiency and gaps in the ideal PHENIX acceptance. In the p+p and d+Au spectra a trigger efficiency correction is also applied.

4.3 Results

The dielectron mass spectra in $s_{NN} = \sqrt{200}$ GeV MB d+Au and Au+Au collisions are shown with their cocktails in Figure 4. The p+p and d+Au spectra agree with the cocktail within the systematic errors. No new cold nuclear matter effects are seen in the MB d+Au dielectron spectrum [19]. The MB Au+Au spectrum contains an enhancement above the cocktail in the low mass region, 0.15-0.75 GeV/c^2, by a factor of $4.7 \pm 0.4(stat) \pm 1.5(sys)$ [16]. Below each of these spectra the ratio of the data to the cocktail is shown. This ratio verifies that the known signals are in good agreement with the cocktail, particularly for the π^0 and the J/ψ where the signal-to-background ratio is large. Often when the π^0 or J/ψ are not in agreement with the cocktail this is the result of incorrect efficiency and dead area corrections that effect the entire spectrum.

The 0-10% Cu+Cu and 0-10% and 10-20% Au+Au show an excess above the cocktail in the low mass region providing information on the onset of the excess [20]. Figure 5 allows for a shape comparison of the excess in 0-10% Cu+Cu and 0-10% and 10-20% Au+Au by overlaying these spectra scaled by $1/N_{Part}$. This excess increases at a rate faster than N^2_{Part} [16].

To further study the dielectron continuum, the mass spectrum is considered in different p_T ranges, as seen in Figure 6. The p+p spectrum at low p_T matches the cocktail well. The MB Au+Au and 0-10% Cu+Cu (not shown) spectra show the majority of the low mass excess is located at low pair p_T. At high p_T and intermediate mass, between the ϕ and J/ψ, the p+p, Cu+Cu and Au+Au data points are above the cocktail with the PYTHIA $c - \bar{c}$ component (solid line) and the cocktail with the randomly associated $c - \bar{c}$ component (dash-dot line). This discrepancy may be because the single electron p_T spectra does not agree with the PYTHIA p_T spectra, because the $b - \bar{b}$ component is not included, or because of additional thermal photon contributions. At low mass and high p_T a slight excess in p+p and larger excesses in the Au+Au and Cu+Cu spectra are seen. Since the mass of the pair is much smaller than the pair p_T, this excess may be attributed to virtual thermal photons that convert into dielectron pairs.

Virtual photons are produced in the same processes that generate real photons. When the mass is much less than the p_T, a virtual thermal photon component follows, $d^2N_{ee}/dm_{ee}dp_T \propto 1/m_{ee}\, dN_\gamma/dp_T$. The thermal photon component is modeled in EXODUS, filtered into the PHENIX acceptance including dead areas and smeared by the PHENIX resolution. The thermal photon contribution is obtained by fitting the data in the mass region, 0.15-0.3 GeV/c^2, for different p_T slices above 1 GeV/c with a combination of the thermal photonic component and the cocktail. This is done for the p+p,

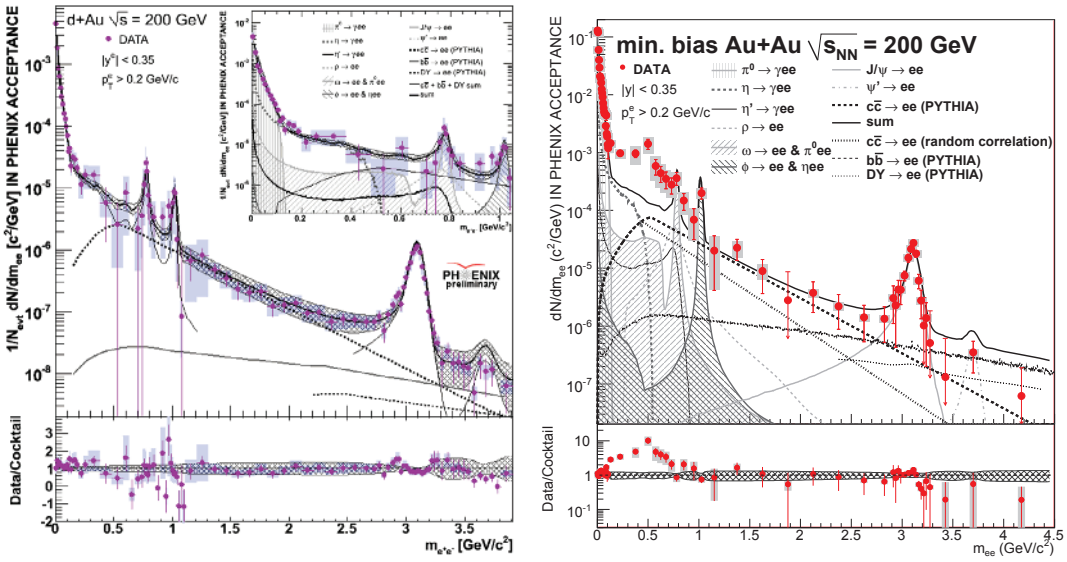

Fig. 4. The MB d+Au and Au+Au dielectron spectra compared to their respective cocktails. Under each plot the ratio of the data to the cocktail is shown.[16][19]

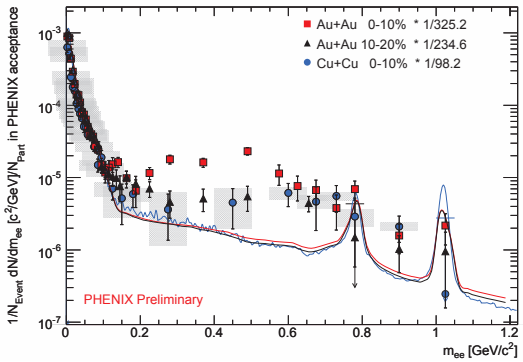

Fig. 5. The dielectron mass spectra for central heavy ion collisions scaled by the inverse of the N_{Part}. The 0-10% Au+Au are shown as red squares, the 10-20% Au+Au are shown as black triangles and the 0-10% Cu+Cu are shown as blue circles. The scaled cocktails for each of these spectra are presented in their respective colors.[16] [20]

d+Au, Cu+Cu and Au+Au spectra. The small excess at low mass and high p_T in p+p collisions is fully described by a direct photon component that is consistent with NLO pQCD calculations. In MB Au+Au the thermal photon measurement is extrapolated to find the initial temperature of the fireball, projecting values of 300 to 600 MeV for thermalization times of 0.6 to 0.15 fm/c respectively [21].

The low mass region of the MB Au+Au dielectron continuum contains more modification than a photonic source can describe. A second source of mass modification exists at low mass and low p_T. The effective temperature of this low mass, low p_T excess can be extracted by fitting the $m_T - m_0$ spectra in the mass region 0.3-0.75 GeV/c^2 after the data has been corrected into the full 2π angular acceptance, as seen in [16]. The m_T spectrum has a kink with a much softer component below 0.6 GeV/c^2 and a harder trend above 0.6 GeV/c^2 corresponding to the two sources of the excess in this mass region. Fitting the low mass m_T spectrum with two exponentials or an exponential plus the thermal photon component results in low effective temperatures of 92.0 ± 11.4 ± 8.4 MeV and $86.5 \pm 12.7^{+11}_{-28.4}$ MeV below 0.6 GeV/c^2. This suggests that the excess below 0.6 GeV/c^2, which is the majority of the excess, is very soft with a low effective temperature[16].

A variety of theoretical comparisons have been made to the MB Au+Au mass, p_T and $m_T - m_0$ spectra including Rapp [22] [23], Dusling and Zahed [24], and Cassing and Bratkovskaya [25] [26]. The Rapp theory describes light vector mesons using the vector dominance model. Dusling and Zahed

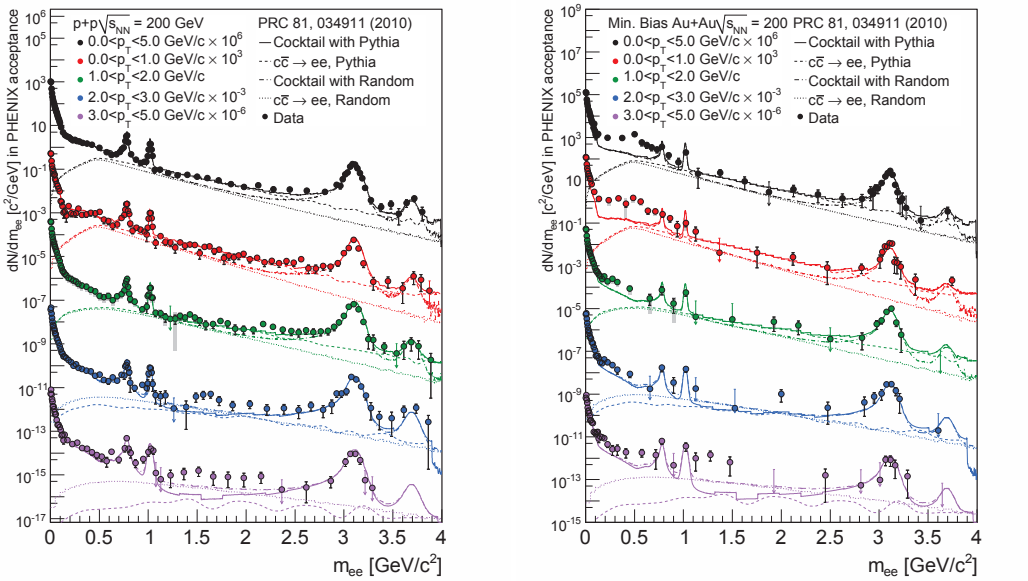

Fig. 6. The dielectron mass spectra of p+p and MB Au+Au in the pair p_T ranges: 0-5 GeV(black), 0-1 GeV/c (red), 1-2 GeV/c (green), 2-3 GeV/c (blue) and 3-5 GeV/c (purple). The data are compared to their cocktail of the hadronic and charm contributions. A second cocktail using a randomly oriented $c - \bar{c}$ contribution is also shown as a dash-dot line.

use a chiral reduction formalism in vacuum and medium modifications are caused by of the hydrodynamic evolution. Cassing and Bratkovskaya applies a microscopic relativistic transport model. None of these theories are able to describe PHENIX's large low mass excess in MB Au+Au, particularly in the low p_T region.

The STAR collaboration has measured the dielectron continuum in p+p and Au+Au collisions [27] [28]. The p+p results are consistent with the STAR cocktail within systematic uncertainty. STAR's MB Au+Au preliminary results have a smaller excess over the STAR cocktail in the low mass region, a factor of $1.53 \pm 0.07(stat) \pm 0.41(sys)$ compared to the cocktail without the ρ meson [28]. One issue when comparing STAR and PHENIX's excesses is the different acceptances in azimuth and rapidity of the two measurements. Another concern is the differences in the respective cocktails. STAR's cocktail excludes the ρ meson, while PHENIX's cocktail includes it. The STAR cocktail uses a much larger the charm cross section, $0.92 \pm 0.10(stat) \pm 0.26(sys)$ mb [27], which is almost twice the amount used in the PHENIX cocktail. These different cocktails are worrisome when interpreting results in the low mass region where the ρ is located and the correlated charm component peaks.

5 Conclusion

The ϕ and ω mesons are suppressed in central and mid-central heavy ion collisions in the p_T ranges 4-7 GeV/c and 4-11 GeV/c respectively. They experience no strong cold nuclear effects in d+Au collisions. In central Au+Au collisions, the high p_T ω and ϕ are suppressed by a factor of five and coincide with the π^0 suppression patterns. This suggests that the meson suppression at high p_T is caused by partonic energy loss. At intermediate p_T, ϕ's are less suppressed than π^0's and agree with K^+ suppression suggesting a recombination production mechanism. Extension of the R_{AA} of the K^+ to higher p_T will shed more light on the ϕ production mechanism. Additionally, measuring the η R_{AA} at intermediate p_T will provide more information on the effect of strangeness enhancement since η mesons have strange quark contributions.

The PHENIX dielectron continuum shows a substantial low mass excess in central Au+Au collisions. The low mass excess is also measured in the most central Cu+Cu collisions and increases at a rate faster than N_{Part}^2 with centrality. While the high p_T, low mass excess is due to thermal virtual photons, the sizable low p_T, low mass excess has yet to be reproduced by theoretical calculations. The p+p and d+Au spectra agree with the cocktail of known dielectron sources suggesting no cold nuclear matter effects. Future measurements in PHENIX include the d+Au dielectron spectra in centrality bins and p+p and Au+Au analyses with the Hadron Blind Detector (HBD) detector. The HBD should improve the signal-to-background in the dielectron analysis by reducing the combinatorial background [29]. To understand the comparison of PHENIX and STAR's results, spectra with the same acceptance and cocktails with the same charm cross section are necessary. PHENIX's silicon vertex detector will help determine the correlated heavy quark contribution from data by identifying off-vertex electrons from open heavy flavor meson decays [30].

References

1. R. Rapp, Phys. Rev. C **63** (2001) 054907
2. R. Arnaldi et al., Phys. Rev. Lett. **96** (2006) 162302
3. A. Adare et al., Phys. Rev. Lett. **101** (2008) 232301
4. A. Adare et al., Phys. Rev. C **82** (2010) 011902
5. A. Adare et al., Phys. Rev. C **83** (2011) 064903
6. J. Adams et al., Phys. Rev. Lett. **92** (2004) 052302
7. J. Adams et al., Phys. Rev. C **71** (2005) 064902
8. K. Adcox et al., Nucl. Inst. and Meth. A **499** (2003) 489
9. M. Aizawa et al., Nucl. Inst. and Meth. A **499** (2003) 508
10. M. Allen et al., Nucl. Inst. and Meth. A **499** (2003) 549
11. A. Adare et. al., Phys. Rev. C **83** (2011) 024909
12. S. S. Adler et. al., Phys. Rev. C **75** (2007) 051902
13. C. Loizides, Eur. Phys. J. C **49** (2007) 339
14. M. Gyulassy, P. Levai and I. Vitev, Phys. Rev. Lett. **85** (2000) 5535
15. A. Adare et. al., Phys. Rev. C **84** (2011) 044902
16. A. Adare et. al., Phys. Rev. C **81** (2010) 02391
17. A. Adare et. al., Phys. Lett. B **670** (2009) 313
18. A. Adare, Phys. Rev. Lett. **97** (2006) 252002
19. Jason Kamin for the PHENIX Collaboration, J. Phys. G: Nucl. Part Phys. **38** 124181
20. Sarah Campbell for the PHENIX Collaboration, J. of Phys: Conf. Series **230** 012034
21. A Adare et. al., Phys. Rev. Lett. **104** (2010) 132301
22. W Lui and R. Rapp, Nucl. Phys. A **796** (2007) 101
23. Ralf Rapp, AIP Conf. Proc. **1322** (2010) 55
24. K. Dusling and I. Zahed, Nucl. Phys. A **825** (2009) 212
25. E. L. Bratkovskaya, W. Cassing and O. Linnyk, Phys. Lett. B **670** (2009) 428
26. O Linnyk, W. Cassing, J. Manninen, E. L. Bratkovskaya and C. M. Ko, arXiv 1111.2975
27. L. Adamczyk et al., arXiv:1204.1809
28. Jie Zhao for the STAR Collaboration, arXiv:1106.6146
29. A. Kozlov et al., Nucl. Inst. and Meth. A **636** (2011) 99
30. Johann Heuser et al., Nucl. Inst. and Meth. A **511** (2003) 210